Available online at www.sciencedirect.com
ScienceDirect
Remote Sensing of Environment 104 (2006) 50–61
Remote Sensing of Environment
www.elsevier.com/locate/rse

Estimation of LAI and fractional cover from small footprint airborne laser scanning data based on gap fraction

Felix Morsdorf [a,*], Benjamin Kötz [a], Erich Meier [a], K.I. Itten [a], Britta Allgöwer [b]

[a] Remote Sensing Laboratories, Department of Geography, University of Zurich, Switzerland
[b] Geographic Information Systems, Department of Geography, University of Zurich, Switzerland

Received 1 May 2005; received in revised form 28 April 2006; accepted 29 April 2006

Abstract

We evaluate the potential of deriving fractional cover (fCover) and leaf area index (LAI) from discrete return, small footprint airborne laser scanning (ALS) data. fCover was computed as the fraction of laser vegetation hits over the number of total laser echoes per unit area. Analogous to the concept of contact frequency, an effective LAI proxy was estimated by a fraction of first and last echo types inside the canopy. Validation was carried out using 83 hemispherical photographs georeferenced to centimeter accuracy by differential GPS, for which the respective gap fractions were computed over a range of zenith angles using the Gap Light Analyzer (GLA). LAI was computed by GLA from gap fraction estimations at zenith angles of 0–60°. For ALS data, different data trap sizes were used to compute fCover and LAI proxy, the range of radii was 2–25 m. For fCover, a data trap size of 2 m radius was used, whereas for LAI a radius of 15 m provided best results. fCover was estimated both from first and last echo data, with first echo data overestimating field fCover and last echo data underestimating field fCover. A multiple regression of fCover derived from both echo types with field fCover showed no increase of R^2 compared to the regression of first echo data, and thus, we only used first echo data for fCover estimation. R^2 for the fCover regression was 0.73, with an RMSE of 0.18. For the ALS LAI proxy, R^2 was lower, at 0.69, while the RMSE was 0.01. For LAI larger radii (~15 m) provided best results for our canopy types, which is due to the importance of a larger range of zenith angles (0–60°) in LAI estimation from hemispherical photographs. Based on the regression results, maps of fCover and LAI were computed for our study area and compared qualitatively to equivalent maps based on imaging spectrometry, revealing similar spatial patterns and ranges of values.

Keywords: Airborne laser scanning; fCover; LAI; Hemispherical photographs; Beam-canopy interaction; Fuel maps

1. Introduction

Robust estimates of vegetation density such as fCover and LAI are critical for a number of applications. They serve as input parameters for biosphere modeling (Bonan, 1993) and play an important role in fire behavior models (Finney, 1998), since they both contain information about a number of relevant ecological processes. LAI was first defined as the total one-sided area of photosynthetic tissue per unit ground surface area (Watson, 1947). This definition is only valid for broad leaf forests though, and consequently Myneni et al. (1997) defined the LAI as the maximum projected leaf area per unit ground surface area. fCover is defined as the fraction of ground covered by vegetation over uncovered ground. Both LAI and fCover are dimensionless parameters, even though LAI is often given as meter square per meter square to illustrate its meaning as an area ratio. Remote sensing has always been assigned a major role in deriving these measures. Many approaches were focused on the retrieval of these parameters from passive optical systems, often by the use of regression models (Cohen et al., 2003; Colombo et al., 2003), and in some cases by using radiative transfer modeling (Koetz et al., 2004; Schlerf & Atzberger, 2006). One limitation of these approaches is the limited characterization of canopy structure, in both horizontal and vertical dimension. Airborne laser scanning (ALS) systems can overcome this shortcoming by penetrating the canopy and revealing the vertical stratification of the canopy, as well as the horizontal structure in case of small-footprint systems providing high point densities. Thus, ALS systems have been widely used for stand-

* Corresponding author.
E-mail address: morsdorf@geo.unizh.ch (F. Morsdorf).

0034-4257/$ - see front matter © 2006 Elsevier Inc. All rights reserved.
doi:10.1016/j.rse.2006.04.019

wise derivation of structural parameters (Lefsky et al., 1999; Lovell et al., 2003; Means et al., 2000), often by means of regression methods choosing some ALS predictor variables (e.g., height percentiles) for ground-based measures of structural information (Andersen et al., 2005; Cohen et al., 2003; Næsset, 2002, 2004). Using small footprint laser data with high point density, the derivation of single tree metrics becomes possible. Its feasibility has been shown by a number of studies (Andersen et al., 2002; Hyyppä et al., 2001; Morsdorf et al., 2004). Some previous studies have already derived LAI and fCover from laser scanning data. Riano et al. (2004) used a relation from Gower et al. (1999) to compute LAI from the gap fraction distribution derived by means of airborne laser scanning, whereas Lovell et al. (2003) used ground-based laser range finder information to model LAI using canopy profiles. Koetz et al. (2006) have used a LIDAR waveform model to invert fCover and LAI from large footprint LIDAR data.

Many small footprint sensors are capable of recording discrete returns (e.g., first and last return, or up to five returns), but not the entire waveform. Small footprint, full waveform sensors are just becoming commercially available. Still, discrete returns contain valuable information about the vegetation density and structure at a high spatial resolution, usually in the order of less than 1 m. It has been shown in a number of studies that first and last returns can be used to model stand properties such as basal area, biomass and LAI. White et al. (2000) have compared different methods for field LAI estimation with airborne laser altimetry, but for a completely different ecosystem compared to the boreal vegetation found in our study area. Our objective is to evaluate the potential of deriving fCover and LAI from discrete return (first and last), small footprint laser data exploiting the information contained in both return types. Our aim is to establish physically meaningful predictor variables and to evaluate their performance with indirect field measurements based on high-precision georeferencing. Emphasis will be placed on differences in viewing geometry between field-based methods and airborne laser scanning. Furthermore, special regard will be paid to the fact that the indirect methods used as ground truth are themselves essentially remote sensing methods.

2. Data

2.1. Site description

The study area for the acquisition of field data is located in the eastern Ofenpass valley, which is part of the Swiss National Park (SNP). The Ofenpass represents a dry inner-alpine valley with rather little precipitation (900–1100 mm/year). Surrounded by 3000 m high peaks, the Ofenpass valley starts at about 1500 m a.s.l. in the west and quickly reaches an average altitude of about 1900 m a.s.l towards the east. The south-facing Ofenpass forests, the location of the field measurements, are largely dominated by mountain pine (*Pinus mugo* ssp. *uncinata*) and some stone pine (*Pinus cembra*), which are of interest for natural succession (Lauber & Wagner, 1996; Zoller, 1992). These forest stands can be classified as woodland associations of Erico–Pinetum mugo (Zoller, 1995).

In Fig. 1 an overview of the test site is given. More than 20% of the stand consists of upright standing dead trees, having a minimum age of 90 years, and mean and maximum ages of 150 and 200 years, respectively.

2.2. Laser scanning data

In October 2002 a helicopter-based ALS flight was carried out over the test area, covering a total area of about 14 km^2. The ALS system used was the Falcon II Sensor developed and maintained by the German company TopoSys. Its sensor specifications are given in Table 1.

The system is a fiber-array laser altimeter recording both first and last intensity peaks from the laser return signal (first/last echo FE/LE). The flight was conducted with a nominal height over ground of 850 m, leading to an average point density of more than 10 points per square meter (p/m^2). A smaller subset of the area (0.6 km^2) was flown at a height of 500 m above ground, resulting in a point density of more than 20 p/m^2, thus combining the two data sets yielded to a point density of more than 30 p/m^2 for both first and last echo. We only used data from the lower over-flight in this study. The footprint sizes were about 0.9 m in diameter for 850 m flight altitude and about 0.5 m in diameter for 500 m altitude. The raw data delivered by the sensor (x,y,z-triplets) were processed into gridded elevation models by TopoSys using the company's own processing software. The Digital Surface Model (DSM) was processed using the first pulse reflections, the Digital Terrain Model (DTM) was constructed using the last returns and filtering algorithms. The grid spacing was 1 m for the large area and 0.5 m for the smaller one, with a height resolution of 0.1 m in both cases. A quality analysis of the raw data was done using six artificial reference targets and is described in detail in Morsdorf et al. (2004). The standard deviations of height estimates based on raw echoes on these targets were as low as 6 cm, with the internal accuracy of the ALS data well below the pixel size of 0.5 m.

2.3. Field inventory

On one hand, the definition of LAI is quite simple, but on the other, its estimation in the field is not trivial at all. There are various ways of determining LAI; a comprehensive summary is given by Jonckheere et al. (2004). Methods can be categorized in two classes, direct and indirect. Direct methods generally use destructive sampling to estimate the total number of leaves on a tree and their area, included angles and distribution to estimate LAI. Indirect methods mostly measure some aspect of the radiative regime and infer the LAI from the distribution of light inside the canopy. Even though the definition of both LAI and fCover is quite different, they are often estimated by the same measurement principle, e.g., LAI2000 or hemispherical photographs, which both can be used to compute LAI and fCover (Jonckheere et al., 2004). We took hemispherical photographs as field samples using a Nikon Coolpix 4500 with a fish-eye lens. The small plot in Fig. 1 shows a canopy height model (CHM) of the area over flown with the lower altitude. Black dots indicate positions where hemispherical photographs were taken in 2002. In 2005, another data collection was carried out

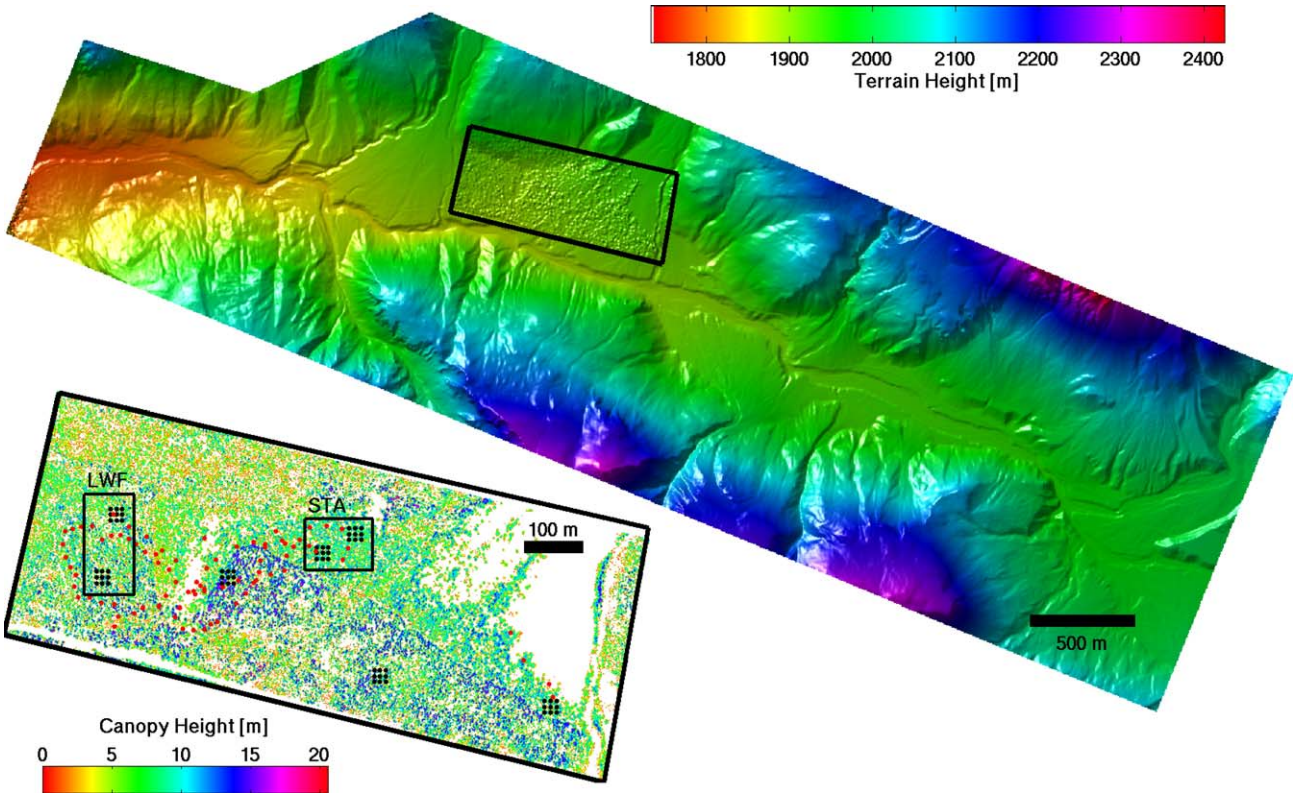

Fig. 1. The Digital Terrain Model (DTM) of the Ofenpass area in the Swiss National Park. The smaller area marked by the black box was sampled with higher point density due to the lower flying height of 500 m above ground. A canopy height map of that area is displayed in the lower left. Black dots mark positions of hemispherical photographs that were taken in 2002 using a handheld GPS for georeferencing. Red dots indicate positions were hemispherical photographs were taken using differential GPS for georeferencing (2005). Black squares mark areas where the histograms in Figs. 2 and 3 were computed from.

at locations marked by red dots. In 2005, a total of 83 hemispherical photographs was taken, and the location of each image was measured using differential GPS equipment. We used three Trimble receivers (one 5700 and two 4700 types) for GPS measurements. One 4700 receiver was set up as base station on a known fixed point of surveying quality inside the study area. The resulting baselines were rather short, between 10 and 600 m in length. The 5700 receiver was used together with a data display (TSCE) to carry out fast static point measurements. A surveying tripod was set up at and leveled at each location, with the GPS antenna placed on top. Succeeding the GPS measurement, the hemispherical photographs were taken. GPS occupation times at each location varied according to satellite availability from 3 to 30 min, and the resulting accuracies based on GPS RMS are in the range of 0.5–5.4 cm with a mean of 1.84 cm. The canopy in our study area was not too dense (medium fCover values of about 40%), thus in most cases occupation times of about 5 min were enough (>5 satellites tracked during measurement), but in the denser parts longer occupation times of up to half an hour were needed to achieve centimeter accuracy.

2.4. Processing of field data

The hemispherical photographs were analyzed using the Gap Light Analyzer (GLA, Frazer et al., 1997) software. Gap fractions were computed for zenith angles from 0° to 90° with 5° spacing, and averaged over all azimuth angles. Areas with sunlight (in about 20 images) were treated separately by a local threshold, before applying a global threshold, as was done for the rest of the images containing no illumination effects due to direct sunlight. LAI was computed for each photograph by GLA's own routines. In coniferous canopies, clumping of small-scale canopy elements (e.g., needles, twigs) into shoots of some centimeters to some decimeters in size manifests an underestimation of LAI that needs to be corrected (Smolander & Stenberg, 2003). Clumping at shoot scale can be addressed by correcting the indirect LAI estimates (often called effective LAI, LAI_{eff}) with a factor depending on the projection function of canopy elements (Weiss et al., 2004). We decided to derive only LAI_{eff}, since a simple coefficient does not alter the quality of our regression. If one needs values for true LAI, one would have to multiply our

Table 1
Specifications of Falcon II sensor platform

Falcon II specifications	
Maximum range	1600 m
Range resolution	2 cm
Scanning angle	±7.15°
Line-scan frequency	653 Hz
Pulse frequency	83 kHz
Laser wavelength	1560 nm
Number of fibers	127
Beam divergence	1 mrad

values by 1.75 (Chen, 1997; Koetz et al., 2004). We applied this correction factor for generating the maps presented in Section 4.5. fCover was derived from the canopy openness measure CO[%] of GLA, which is based on the fraction of sky pixels weighted with hemispherical area by Eq. (1)

$$\mathrm{fCover} = 1 - \mathrm{CO} \tag{1}$$

Only pixels from zenith angles smaller than 10° were used for the estimation of fCover, as was proposed by Weiss et al. (2004).

3. Methods

3.1. Derivation of fractional cover from laser data

The Toposys Falcon II system is capable of recording a first and a last echo of the return signal. A first echo will be triggered if the return signal reaches a certain intensity; hence, the vegetation cover reaches a critical density and/or reflectivity. If the vegetation is not too dense, a part of the beam can further penetrate the canopy, until the threshold for the intensity is surpassed a second time and the so-called last echo is triggered. Depending on the vegetation openness and density, this can be on the ground or inside the vegetation. A minimum distance needs to be between the first and last echo for their separation, which depends on the pulse duration of the laser emitter. With a system recording first and last echo, three types of returns scenarios are possible:

- first echo
- last echo
- single echo, first echo=last echo

The term *single echo* describes the case where only one echo is triggered from a return signal, resulting in both values having the same height. Most single echoes will come from plain surfaces such as roads or generally from the ground, but there are some in the vegetation, as will be discussed in the Section 4.1.

For each of the three return classes, we computed fCover according to Eqs. (2) and (3).

$$\mathrm{fCover} = \frac{\sum E_{\mathrm{vegetation}}}{\sum E_{\mathrm{total}}} \tag{2}$$

with

$$E_{\mathrm{vegetation}} = E_{\mathrm{total}} > 1.25\ \mathrm{m} \tag{3}$$

$E_{\mathrm{vegetation}}$ and E_{total} denotes vegetation echoes and all (ground and vegetation) echoes respectively. We chose a height threshold of 1.25 m, since this was the height at which the lens was placed when taking the hemispherical photographs.

The value of fCover for first pulse data is larger than that for single echoes, which in turn is larger than the value for last echoes, as can be seen in Figs. 2(b) and 3(b). Lovell et al. (2003) concluded from similar findings that the *real* value of fCover must satisfy the following condition:

$$\mathrm{fCover_{FE}} > \mathrm{fCover} > \mathrm{fCover_{LE}} \tag{4}$$

FE and LE denote first echo and last echo, respectively. Based on Eq. (4) one can state that using first pulse information for fCover estimation will overestimate the true fCover value, whereas using last pulse information will underestimate true fCover. The value of true fCover lies somewhere in between, but where

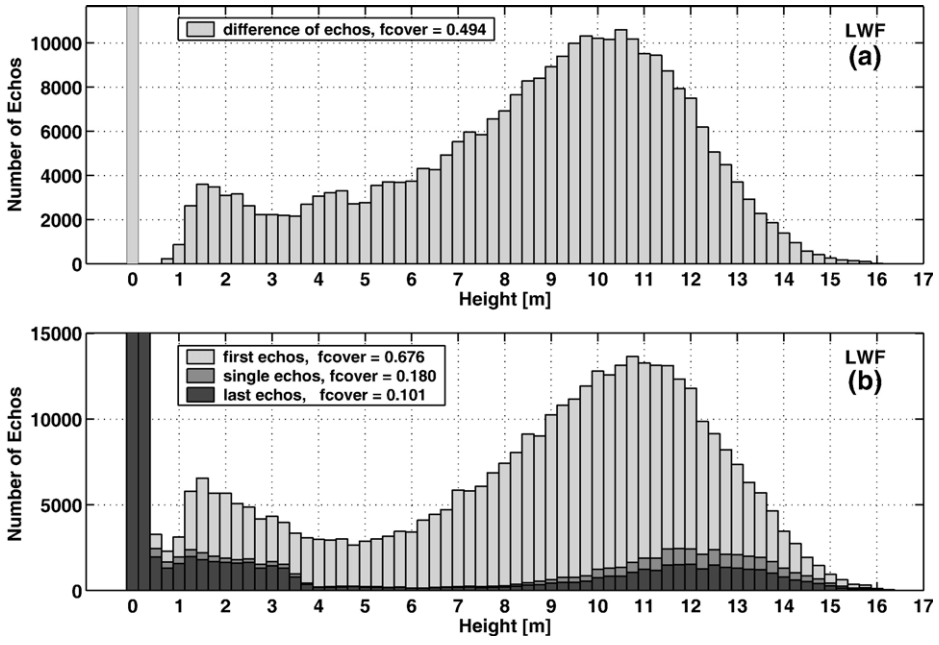

Fig. 2. Histogram of difference of first and last pulse (a), histogram of first, last and single echoes (b) for site LWF. Note that limits of the *y*-axis have been lowered for better visibility of the vegetation part of the histogram, and thus, the percentage of last/single echoes to first echo and the absolute number of ground echoes cannot be drawn from this graph.

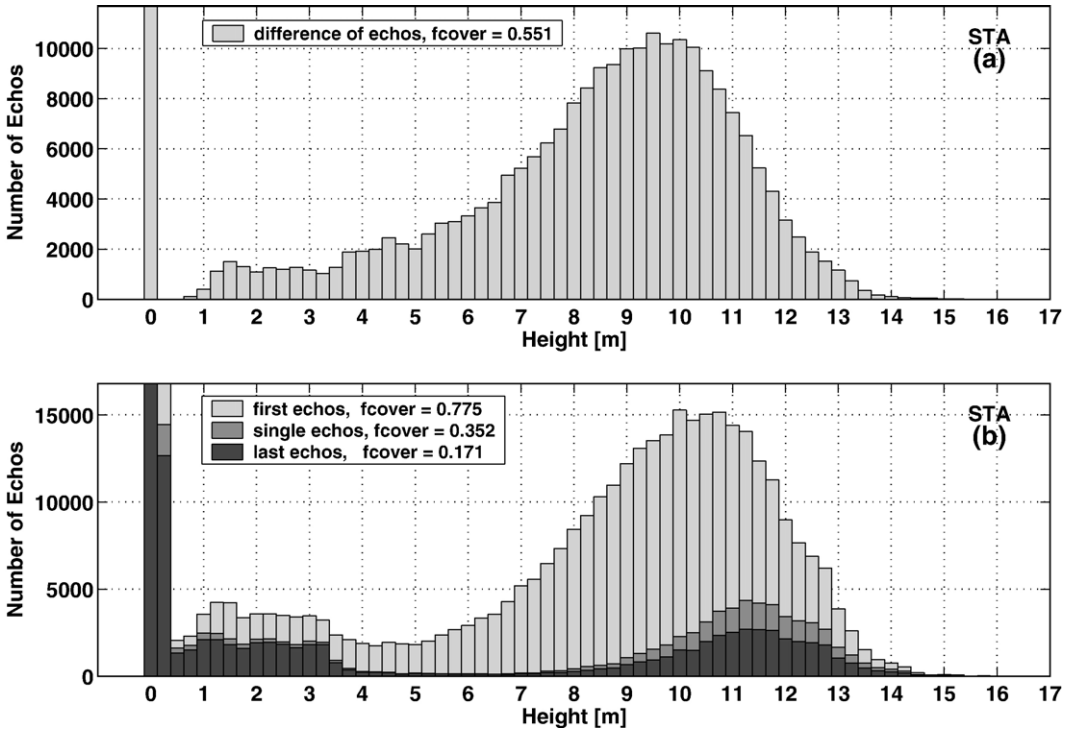

Fig. 3. Histogram of difference of first and last pulse (a), histogram of first, last and single echoes (b) for site STA. The heights have been subtracted by terrain heights interpolated to raw data coordinates from the digital terrain model Toposys provided.

exactly is difficult to ascertain, as it will depend on vegetation type/condition and sensor specifications. Many studies deriving stand level indices have only used first pulse data (Yu et al., 2004), since the separation mechanism is not well understood, and still the most significant information is contained in a first pulse histogram. As, e.g., Holmgren and Persson (2004), we compute fCover from first and last returns separately by thresholding vegetation heights according to Eqs. (2) and (3). Following this, we use single and multiple regressions of these two fCover values to determine their influence on true fCover as determined by field measurements. Furthermore, we will compute fCover for circular ALS raw data patches (data traps) of 2–25 m in diameter.

3.2. Derivation of LAI from laser data

Our goal is to establish a predictor variable of LAI that is closely linked to the way LAI is estimated using the indirect methods in the field. Following Weiss et al. (2004), the LAI can be expressed through the following equation. The leaf area index, L, at a level H in the canopy is related to the leaf area density $l(h)$ through

$$L = \int_0^H l(h)\mathrm{d}h \tag{5}$$

If we introduce the contact frequency $N(H, \theta_v, \phi_v)$ we can write Eq. (5) as follows:

$$N(H, \theta_v \phi_v) = \int_0^H G(h, \theta_v \phi_v) \frac{l(h)}{\cos\theta_v \mathrm{d}h} \tag{6}$$

θ_v and ϕ_v denote viewing zenith and azimuth angle, respectively, and $G(h, \theta_v, \phi_v)$ the projection function. If leaf area density and projection function are considered independent of the level h in the canopy Eq. (6) can be simplified into Eq. (7):

$$N(L, \theta_v, \phi_v) = G(h, \theta_v, \phi_v) \frac{L}{\cos\theta_v} \tag{7}$$

Considering the Falcon II system with its maximum scanning angle of 7.1°, $\cos\theta_v$ is only changing up to 0.75% from 1 and can thus be neglected. As we have solely conifers in our study area, the projection function is set to 0.5 assuming a spherical foliage distribution (as in Sun & Ranson, 2000; Koetz et al., 2004); thus, we yield a direct proportional relationship of contact frequency to LAI:

$$N(L) = 0.5 * L \tag{8}$$

The contact frequency itself should be linearly related to the distribution of first, single and last echoes inside the canopy. We still need to account (calibrate) for specific instrument characteristics, which will be footprint size (depends on beam divergence and flying height) and the thresholding algorithm for detection of first and last pulse, as well laser beam attenuation through the atmosphere. In this study, we are using a linear regression model to do so.

Based on the concept of contact frequency we propose to compute a LAI proxy from ALS data by

$$N_{\mathrm{LAI}} = \frac{\sum E_{\mathrm{FE}}}{\sum E_{\mathrm{LE}} + E_{\mathrm{SE}}} \tag{9}$$

E_{FE}, E_{SE} and E_{LE} denote the three types of returns described in detail in Section 3.1, but only for crowns. The vegetation returns are classified by thresholding the height over terrain of the raw laser hits with a value of 1.25 m, according to the estimation of fCover in Eq. (3). The hypothesis for this proxy is as well based on results displayed in Figs 2(b) and 3(b). As for fCover, we will compute this LAI proxy for circular ALS data traps of 2–25 m in diameter.

Dispersion of crowns inside the canopy is not an issue for our approach, since we only compute the fraction of returns from greater than 1.25 m above the ground, thus, inside the canopy. This is a valid approach, since our study site is a single layered and almost a single species canopy type. Thus, our contact frequency measure is only derived from crowns, due to the ability of high point density, small footprint laser scanner data of spatially resolving single tree crowns (Morsdorf et al., 2004). In order to compare these ALS-derived estimates of canopy LAI with indirect field measurements, we need to correct for the distribution of canopy elements (e.g., trees) in the scene, which will be done by using the ALS derived fCover values. Since the LAI estimated by ALS is only estimated for the canopy, we need to multiply that LAI value with the respective value of ALS derived fCover in order to yield an LAI estimation for the whole data trap. For instance, if the *canopy* LAI (LAI only computed from canopy elements) was 4 and the fCover value of that respective scene 0.5, then the real LAI for the scene would be 2. Hemispherical photographs only measure the scene LAI and fCover, since they cannot discriminate between gaps within crowns and gaps between neighboring crowns.

$$N_{\mathrm{LAI,scene}} = N_{\mathrm{LAI,canopy}} * \mathrm{fCover}_{\mathrm{scene}} \tag{10}$$

Still, we need to assume horizontal and vertical uniform leaf angle and leaf property distribution. One leaf property that could alter this way of LAI estimation is leaf reflectance. The difference of reflectance between ground and canopy needs to be considered as well. This reflectance difference reveals a major caveat regarding the comparability of laser-based vegetation indices from different stands and possibly even different sites. We will discuss its influence in greater detail in the following section.

3.2.1. Vegetation reflectance considerations

Based on field measurements, the foliage reflectance at 1560 nm (wavelength of laser beam) is 21.5%, whereas the background reflectance of the under-story is 15.2%, making up for a ratio of 1.4. This ratio is specific for our study area and can be considered a constant for our area, due to the homogeneity of the canopy and under-story in respect to plant species. In order to assess the feasibility of our approach regarding the assumption on spatially uniform reflectance of the canopy, we conducted some tests using PROSPECT (Jacquemoud & Baret, 1990), modeling the reflectance of the green canopy elements in our study site using average leaf parameters from field measurements collected at different sites (Koetz et al., 2004). We varied the moisture content within a range observed in the field, as at 1560 nm absorption due to moisture is the dominant effect. Simulated leaf reflectance yielded 20.8% reflectance for the lowest values of moisture and 19.2% for the highest value observed, making up for an absolute difference of only 1.6%. This is small enough to be neglected, considering results from a practical test using artificial targets on object visibility using different reflectances (Wotruba et al., 2005). All other parameters of PROSPECT were left constant, since our test site is predominantly covered by only one tree type, which is mountain pine.

3.3. Regression methods

For all regressions in this paper, adjusted R^2 and RMSE were computed by the following equations (see Kvalseth, 1985, for details):

$$R^2 = 1 - \frac{n-1}{n-p}\frac{\sum(y-\hat{y})^2}{\sum(y-\bar{y})^2} \tag{11}$$

n is the number of samples, p is the number of parameter in the regression model (which is two for all our presented regressions), $\hat{y}$ is the fitted value of a sample y (e.g., LAI) and $\bar{y}$ is the mean of all y's. The root mean square error is calculated as

$$\mathrm{RMSE} = \sqrt{\frac{\sum(y-\hat{y})^2)}{n-p}} \tag{12}$$

For each of the regressions, we excluded outliers in a first linear regression, where the 5% confidence interval for the residuals was estimated and values not enclosing zero were flagged (see Chatterjee & Hadi, 1986, for details). We still include them in the regression graphs as empty circles, in order to illustrate that they are real outliers. These outliers may originate from temporal differences between LIDAR flight and field data collection, but more likely is that they originate from errors in the acquisition/processing chain of hemispherical photographs, be it by thresholding errors or illumination differences.

4. Results

4.1. Height histograms

In Figs. 2 and 3 are large area histograms of the measured vegetation heights of three echo types depicted. These height distributions are either called *modeled waveform* in literature (Riano et al., 2003) or canopy density, as in many other studies. Colored in medium and darker gray, the last and single echoes are (if not on ground) mostly concentrated in the upper canopy, with their maximum just before the maximum of total echoes. Histograms have been derived from areas with different vegetation densities called LWF (Fig. 2) and STA (Fig. 3). Their geographical extent is marked by black rectangles in Fig. 1.

When comparing the two sites LWF and STA, one can note that the fraction of last and single echoes in the upper canopy and lower canopy is higher for STA than for LWF, with the mean LAI from field measurements equaling about 1 at LWF and about 2 at STA. This supports our hypothesis that LAI can be estimated by the fraction of different return types inside the canopy. From the upper panels of these figures, we can also read off the approximate instrument dead-time, which is the

minimum vertical distance required between two objects to be separately detected by first and last echo. This minimum distance is approximately 1 m, which can be seen in Figs. 2(a) and 3(a). There, a height distribution of the difference of first and last echo is shown, and one can clearly notice the gap from zero to near the 1 m bin. This minimum distance is due to the laser pulse duration. As our typical crown height is between ~3 and 8 m, we should be able to receive separated echoes (first/last) from the crowns in most cases.

4.2. Scales of correlation

If both ground measurements and airborne data are georeferenced to within less than 1 m, one can assign each hemispherical photograph an area of ALS raw data for the LAI and fCover derivations. Since one does not know how far the hemispherical photograph can "see", we needed to have an estimate of how large the diameter of ALS data has to be chosen around the position of the hemispherical photograph in order to get good agreement of field estimates and the respective ALS ones. Thus, we computed fCover for patches (or traps) from 4 to 50 m diameter according to Eq. (2). These patches have also been called *data traps* in literature (Lovell et al., 2003). We varied also the zenith angles, since we did not really know which zenith angles of hemispherical photographs would capture the information contained in these patches. The distance range that the hemispherical photographs can sample will depend on the vegetation density in the horizontal dimension and on vegetation density and canopy height in the vertical dimension.

In Fig. 4 we display a matrix containing the R^2 values for each regression of field and ALS estimates of gap fraction (which in case of ALS is fCover), varying ALS data trap size (x-axis) and zenith angle of hemispherical photograph (y-axis). From this figure, it is evident that significant correlation (as denoted by R^2 values >0.6) occur for all zenith angles from 0° to 65° and for 1 to 25 m in radius of ALS raw data patch. For smaller zenith angles, the correlation is high only for small data trap sizes, whereas for larger trap sizes there is only high correlation for large zenith angles. Especially, at very small zenith angles of less than 10°, there is a significant linear relationship of gap fraction with ALS data at trap sizes of up to 2 m in diameter. This shows that the georeferencing was sufficient in order to link the data at such small scales. For each zenith angle, we computed the required data trap size to capture the complete field of view of a hemispherical photograph for a defined canopy height. This should work under the assumption that the canopy is not too dense, and thus limit the distance a hemispherical photograph will be able to "look". Using the values of 6 m and 13 m as lower respective upper bounds for canopy height, a trigonometric curve was computed and included in the Fig. 4 as black and grey lines. The maxima of correlation ($R^2>0.6$) are in good agreement with these lines, with some regression models having an R^2 as high as 0.8.

4.3. fCover

For the derivation of fCover from hemispherical photographs only the innermost zenith angles up to 10° should be used according to Weiss et al. (2004). The zenith angles up to 10° have the highest correlation with data trap sizes of radii up to 2 m, as can be seen at the axis-crossing in the upper-left corner of Fig. 4. Thus, we computed fCover from ALS data traps sized 4 m in diameter for each first and last echo data separately. Fig. 5 contains the regressions of these ALS derived fCover values with the respective field measurements. The upper panel contains the fCover value computed from first echo data, the lower the respective one for last echo data. The R^2 for the first echo data is 0.73, with the RMS of 0.18. The R^2 for the last echo regression is lower than that for the first echo data (0.36, with an RMS of 0.11). By comparing the regression lines with the one to one line (thick black one), one can note as well that first echo data will overestimate true fCover, whereas last echo data will underestimate. A multiple regression for both last echo and first echo-based fCover against field measured values was carried out as well. There was no increase of R^2 (remained at 0.73) over the solely first echo-based regression. Thus, we used the regression model based on first echo data for the computation of fCover values in Fig. 8. There seems to be more noise attributed to the lower values, especially in the regression of first echo derived fCover. Higher values are generally less distributed about the regression line. It is also evident that a lot of last echo derived fCover values are zero, while the hemispherical photographs still produced values greater than zero. This is an effect of vegetation being transparent in respect to last echo returns to some extent, depending on vegetation density.

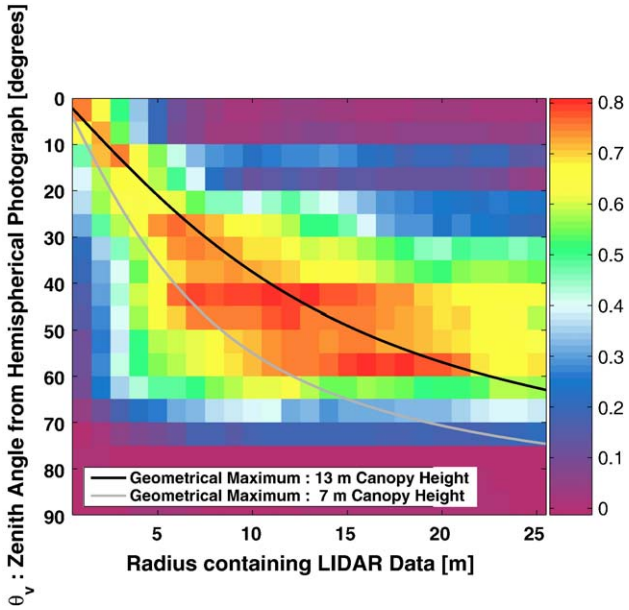

Fig. 4. Matrix of coefficients of determination (R^2) for regression of field measured gap fraction and ALS derived fCover for a range of zenith angles and ALS raw data patch sizes. The theoretical line of maximum correlation was plotted as well for two different canopy heights.

4.4. LAI

The same procedure was carried out for the LAI proxy, but we could not vary the zenith angles GLA uses to compute LAI from. GLA offers either an *LAI 5 Ring* value, integrated from zenith angles of 0–75° or an *LAI 4 Ring* value, which is integrated from

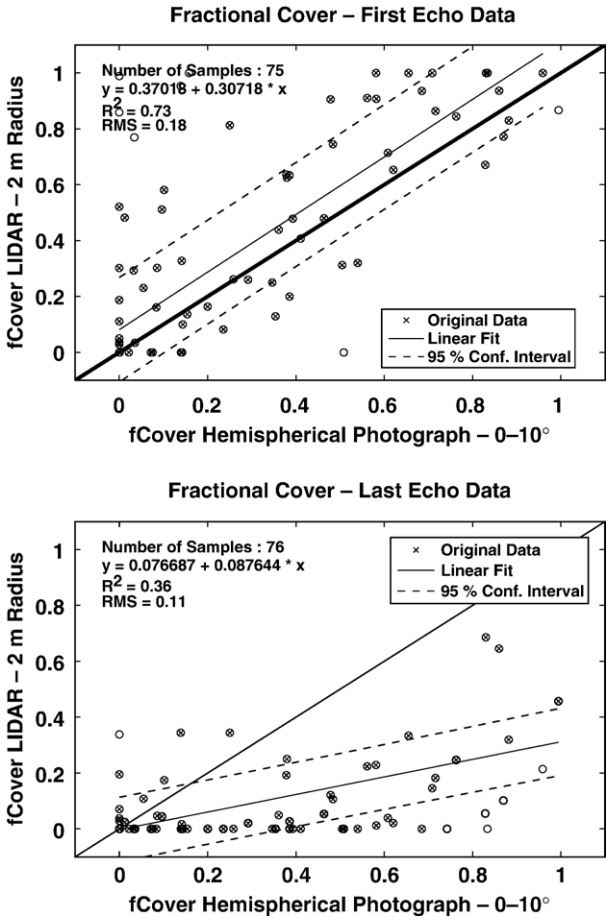

Fig. 5. Regression of ALS derived fCover with respective values computed from hemispherical photographs. Upper panel shows regression for first echo data, lower shows regression for last echo data. Red circles denote outliers, which have not been used for the statistic computations.

zenith angles of 0–60°.We used the latter for the regressions presented in this paper. Thus, we can only provide the dependency of the LAI regression relative to the size of laser raw data patch, which is depicted in Fig. 6. The values of R^2 are as low as 0.1 for patches of 2 m in radius and reaches a maximum of about 0.65 at about 15 m in diameter. For larger radii than that, R^2 decreases to values below 0.5. Thus, we chose a diameter of 30 m for the LAI regression in Fig. 7.

In Fig. 7 the regression of ALS derived LAI and field measured (hemispherical photographs) is depicted. R^2 is 0.69, with an RMS of 0.01. The regression model coefficients are used to compute LAI for the maps in the following section. The number of samples used for the LAI regression is 52, since we excluded all images where the influence of direct sunlight was visible. It is also visible that the spread of values (hence, noise) about the one-on-one relation is higher for larger LAI values, resulting in a behavior opposite of what was observed for fCover in Fig. 5.

4.5. Maps of LAI and fCover

Using the regression models, we computed maps for both LAI and fCover for the small study area. For a qualitative comparison, we placed these maps side by side with maps derived by imaging

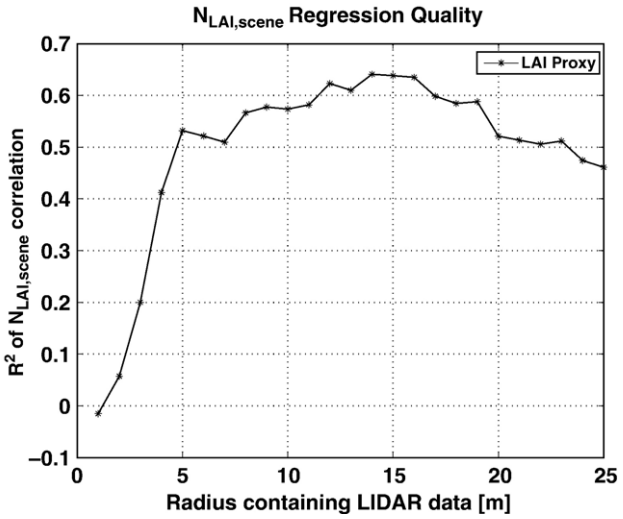

Fig. 6. Coefficient of determination (R^2) for LAI proxy regression for a range of ALS raw data patches.

spectroscopy using radiative transfer modeling (Koetz et al., 2004). The imaging spectrometer data set has been acquired by the sensor DAIS7915 in the summer 2002 over SNP in a geometric resolution of 10 m matching the one of the ALS (Chang, 1993). The inversion of the coupled radiative transfer models PROSPECT and GeoSAIL provided biophysical vegetation properties including LAI and fCover (Huemmrich, 2001; Jacquemoud & Baret, 1990). The maps are depicted in Fig. 8, with the results from ALS on the left side and the respective results from imaging spectrometry on the right side. The LAI in the lower left plot is the unclumped, true LAI, which was calculated by multiplying the values of LAI_{eff} (as estimated using our regression model) by 1.75 (Koetz et al., 2004). One can note that values appear to be in the same range for both LAI and fCover as derived by both methods. The spatial patterns are more or less the same for both methods, with high LAI and fCover values towards the large

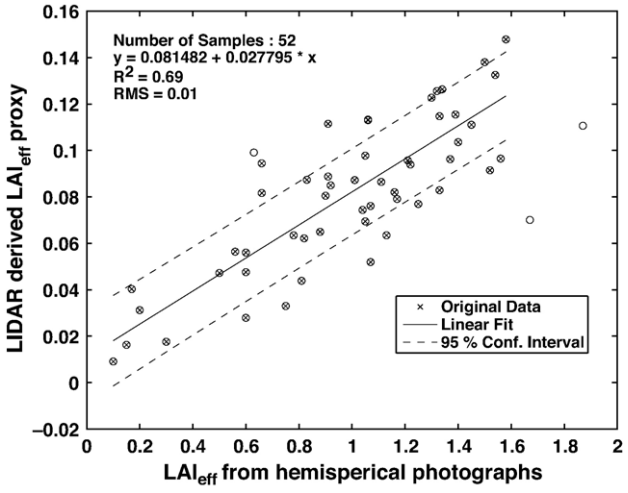

Fig. 7. Regression of ALS derived LAI Proxy $N_{LAI,scene}$ with LAI_{eff} from hemispherical measurements. Processing of hemispherical photographs was done using GLA. Red circles denote outliers, which have not been used for the statistic computations.

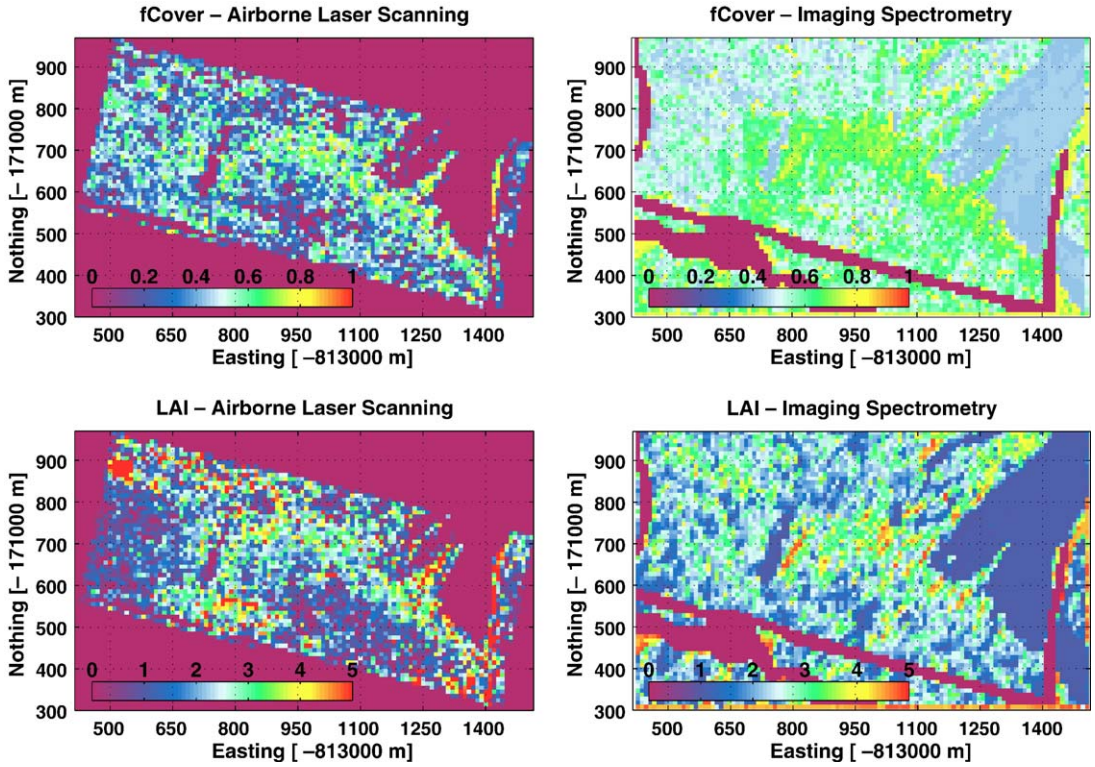

Fig. 8. Maps of fCover and LAI for the small study area (black square in Fig. 1) derived both from airborne laser scanning and imaging spectrometry. The pixel size in each case is 10 m. Note that for imaging spectrometry areas containing non vegetated surfaces (road, river bed) have been masked out.

alpine meadow on the right hand side. There are some differences, though. For ALS, the alpine meadow, road or river-bed areas are correctly assigned a tree LAI and fCover of 0. For the imaging spectroscopy approach forest and meadow areas would need to be identified and separated a priori since the employed radiative transfer model cannot distinguish between these surface types. A standard land surface type classification based on the spectral information content of the imaging spectrometer data could be used to mask out non-forest surface types.

Comparing fCover and LAI, high LAI values are visible especially at the edges of forest or close to gaps, where the vegetation has better environmental conditions. However, the larger spatial patterns are similar to the map of fCover. This is due to the fact that other ecological parameters control the healthiness and distribution of the vegetation. The spatial patterns of these parameters and processes are then *masked* into the maps of LAI and fCover.

5. Discussion and conclusions

In the past years, airborne laser scanning has been established as a valuable tool for forest structural analyses. Algorithms for the derivation of properties such as tree height, biomass and basal area have been implemented and evaluated on various study sites using laser data from both small and large footprint systems. Our aim was to show the potential of small footprint laser data for the derivation of fCover and LAI, using only single and possibly physical meaningful ALS predictor variables. As was found in previous studies, we could show that it is possible to estimate fCover from ALS data by using the fraction of vegetation echoes over ground echoes as a predictor variable. fCover was computed from both first and last echoes using a data trap size of 2 m radius, with R^2 higher for first echo data (0.73) and lower for last echo data (0.36). First echo-based fCover values will overestimate field measured values, whereas last echo-based fCover values will underestimate them. However, we found that first echo-based fCover data is sufficient in establishing a link with field data, and that adding the last echo-based fCover values into a multiple regression did not improve R^2. Thus, an overestimation of ALS data is visible and needs to be corrected, e.g., through the use of a regression model as was done in our study. It is known that fCover estimates by hemispherical photographs are biased upwards due to the viewing geometry (Lovell et al., 2003; Weiss et al., 2004), which will produce a lot of vegetation pixels by stems. Thus, one could argue that the ALS would provide a truer estimate of fCover, based on its nearly optimal viewing geometry (near-nadir view). It should be noted that because of our scanner's small scanning angle of 7.15°, we were able to neglect its influence on our results. For larger scanning angles (up to 30°) our findings may not be valid. Significant noise was visible in our regression, leading to somewhat lower R^2 values. One source of this noise could be attributed to the difference in viewing geometry of ALS data and hemispherical photographs. For the lower values the noise is more prevalent than for the higher values, which could be explained by heterogeneity effects in the lower density canopy of the STA site. This is where most of the lower values originate from. There are also many high laser values assigned with hemispherical values of zero. A high spatial sampling density is needed

to get robust fCover estimates in medium dense and heterogeneous canopies, since the area up to 10° off nadir will in most cases contain sky. This is probably due to the sampling strategy, where the camera is not placed too close to a tree to avoid overestimation due to stems and for practical considerations. For sparse coniferous canopies such as those present on our test site, there is a high proportion of sky within the first 10° of zenith angle. However, ALS systems can provide a much better horizontal sampling of the forest canopy than field inventory methods such as hemispherical photographs.

We have tried to show that the fraction of different return types inside the canopy acts as a new and direct predictor variable for LAI. Regression of the ALS estimates with field data from hemispherical photographs showed moderate to good agreement, with an R^2 of 0.69 and an RMS of 0.01. For LAI, the ALS data trap size showing best correlation with hemispherical photographs was 15 m in diameter, much larger than the one used for fCover. This is explained by GLA using all zenith angles from 0° to 60° for its LAI_{eff} computation.

However, an instrument and vegetation type specific calibration parameter will have to be applied to the ALS derived estimates in any case. The vegetation specific parameter will probably be influenced by two factors, i.e., reflectance differences and clumping of canopy elements at smaller scales than footprint size. Clumping is a well studied phenomenon, since it needs to be corrected for most field-based methods as well (e.g., LAI2000, hemispherical photographs, ceptometer, Jonckheere et al., 2004). Correction factors have been derived for various canopy types that are used in day-to-day field work. Hence, it would not be too big of a problem to extend their use to ALS data. Canopy reflectance, though, is an issue that requires a more complicated procedure. For ALS-LAI_{eff} estimates to be inter-comparable, the reflectance of canopy elements in the wavelength of the laser (the ALS system used provides 1560 nm) should be roughly the same. Modern ALS systems allow as well the recording of the intensity of the returned signal, so this information could be used for assessing effects of canopy reflectance differences. Unfortunately, this option was not yet available in 2002 when our flight campaign was carried out. The processing of hemispherical photographs involves the process of manually thresholding images, a potential source for biases and random noise. Nobis and Hunziker (2005) have tried to overcome this by using automatic thresholding. A very common feature of LAI derived from passive remote sensing data is the saturation for high values (Colombo et al., 2003; Koetz et al., 2005). Our approach seems to be capable of returning effective LAI values above 4 (see Fig. 8). Further research is needed to determine whether this finding is robust.

A systematic error that could also explain the noise present in our regressions may be the inability of the hemispherical photographs to separate between-crown and within-crown gap probabilities, which they cannot discriminate. By comparison, the small-footprint ALS can do this to an certain extent. There is some ambiguity regarding laser returns from the edges of trees, which could be misclassified as full crown hits. Their ratio of first to single/last echoes would not be representative for the within-crown-gap probability. A more sophisticated treatment of the three return classes to retrieve LAI, instead than just taking the fraction of first to single and last returns could also improve the results. It might be that the single returns are more sensitive to LAI changes and vice versa, depending on vegetation type and thresholding used. It would be beneficial to have instruments that deliver intercomparable results for LAI and fCover from very different areas. This can only be achieved by taking the radiative regime and the associated physical processes into account. We have tried to take a step in that direction by choosing direct, physically meaningful metrics of ALS raw data for LAI and fCover.

Comparing our results with findings from imaging spectrometry from the same test area, we found good agreement in spatial patterns, but also a systematic overestimation of canopy fCover by imaging spectrometry in areas were only few to no trees were situated. Thus, ALS does provide a truer estimate of canopy fCover in these regions. Furthermore, areas which do not contain vegetation of a certain height do not need to be masked out manually; a simple threshold will do. The high-resolution maps of fCover and LAI could have a great potential for forest structural analysis, but so far, they have not been applied to tasks such as habitat analysis or other ecological problems, with exception of the work of Hill et al. (2004), where the potential of ALS data for bird habitat quality assessment was studied.

We have found that the absolute values of fCover are highly dependent on the size of LIDAR raw data trap, similar to findings by Lovell et al. (2003). This effect is dependent on the size and spatial distribution of canopy elements (e.g., trees). For a completely homogeneous canopy there should be no scale dependency of fCover above a certain granularity scale, e.g., in case of a corn field data traps larger than about 1 m should not vary significantly in their fCover values. Combined with methods for single tree extraction (Hyyppä et al., 2001; Morsdorf et al., 2004), the work we presented would allow the direct retrieval of a close to "true" foliage profile from airborne laser scanning data (Lovell et al., 2003; Ni-Meister et al., 2001). This is due to the fact that between-crown and within-crown-gap probability can be discriminated. This combination of the two approaches will be a subject of future work. Only the small-scale clumping on scales smaller than footprint size needs to be corrected, whereas crown dispersion is actually known due to high point density and small footprint size of the laser scanner used in this study. The downside of small footprint laser scanning is its relatively high costs, which would impede a campaign over a greater area only for, e.g., LAI retrieval. But since these systems offer many other benefits (e.g., precise terrain models, forest boundaries, the ability of deriving single tree characteristics), the cost per feature will decrease. Currently, the country of Switzerland is being scanned by a small footprint laser scanner up to heights of 2000 m AGL. This will be a valuable multi-purpose data set, where LAI and fCover could be additional features. Further studies, possibly including radiative transfer modeling of single scenes could aid in further investigating the relationships we established and how robust they are with respect to different site conditions and sensor specifications. Of special interest would

be differences in canopy reflectance and different ALS system configurations. Some of these ALS specific parameters that most probably have an influence on the metrics we used are flying height (footprint size, point spacing), laser wavelength and incidence angle.

Acknowledgments

This project is funded by the EC project "Forest Fire Spread and Mitigation" (SPREAD), EC-Contract No. EVG1-CT-2001-00027 and the Federal Office for Education and Science of Switzerland (BBW), BBW-Contract No. 01.0138.

References

Andersen, H. -E., McGaughey, R. J., & Reutebuch, S. E. (2005). Estimating forest canopy fuel parameters using lidar data. *Remote Sensing of Environment*, *94*(4), 441–449.

Andersen, H. -E., Reutebuch, S. E., & Schreuder, G. F. (2002). Bayesian object recognition for the analysis of complex forest scenes in airborne laser scanner data. *ISPRS Commission III, Symposium 2002* September 9–13, 2002, Graz, Austria A-035 ff (7 pages).

Bonan, G. B. (1993, Mar.). Importance of leaf area index and forest type when estimating photosynthesis in boreal forests. *Remote Sensing of Environment*, *43*(3), 303–314.

Chang, S. -H., Westfield, M. J., et al. (1993). 79-channel airborne imaging spectrometer. *Im. Spec. of the Terr. Env., SPIE*, *Vol. 1937* (pp. 164–172).

Chatterjee, S., & Hadi, A. (1986). Influential observations, high leverage points, and outliers in linear regression. *Statistical Science*, *1*(3), 379–416.

Chen, J. M., Rich, P. M., et al. (1997). Leaf area index of boreal forests: Theory, techniques, and measurements. *Journal of Geophysical Research—Atmospheres*, *102*(D24), 29429–29443.

Cohen, W. B., Maiersperger, T. K., Gower, S. T., & Turner, D. P. (2003). An improved strategy for regression of biophysical variables and landsat etm+ data. *Remote Sensing of Environment*, *84*(4), 561–571.

Colombo, R., Bellingeri, D., Fasolini, D., & Marino, C. M. (2003). Retrieval of leaf area index in different vegetation types using high resolution satellite data. *Remote Sensing of Environment*, *86*(1), 120–131.

Finney, M., 1998. Farsite: Fire area simulator-model. development and evaluation. USDA Forest Service Research Paper RMRS-RP-4.

Frazer, G., Trofymow, J., & Lertzman, K., 1997. A method for estimating canopy openess, effective leaf area index and photosynthetically active photon flux density using hemispherical photography and computerized image analysis techniques. Tech. rep., Information Report BC-X-373, Natural Resources Canada, Canadian Forest Service, Pacific Forestry Centre, Victoria, BC.

Gower, S. T., Kucharik, C. J., & Norman, J. M. (1999). Direct and indirect estimation of leaf area index, fapar, and net primary production of terrestrial ecosystems. *Remote Sensing of Environment*, *70*, 29–51.

Hill, R., Hinsley, S., Gaveau, D., & Bellamy, P. (2004). Predicting habitat quality for great tits (parus major) with airborne laser scanning data. *International Journal of Remote Sensing*, *25*, 4851–4855.

Holmgren, J., & Persson, A. (2004). Identifying species of individual trees using airborne laser scanner. *Remote Sensing of Environment*, *90*, 415–423.

Huemmrich, K. F. (2001). The geosail model: A simple addition to the sail model to describe discontinuous canopy reflectance. *Remote Sensing of Environment*, *75*(3), 423–431.

Hyyppä, J., Kelle, O., Lehikoinen, M., & Inkinen, M. (2001). A segmentation-based method to retrieve stem volume estimates from 3-D tree height models produced by laser scanners. *IEEE Transactions on Geoscience and Remote Sensing*, *39*, 969–975.

Jacquemoud, S., & Baret, F. (1990, Nov.). Prospect: A model of leaf optical properties spectra. *Remote Sensing of Environment*, *34*(2), 75–91.

Jonckheere, I., Fleck, S., Nackaerts, K., Muys, B., Coppin, P., Weiss, M., et al. (2004). Review of methods for in situ leaf area index determination: Part I. Theories, sensors and hemispherical photography. *Agricultural and Forest Meteorology*, *121*(1–2), 19–35.

Koetz, B., Baret, F., Poilve, H., & Hill, J. (2005). Use of coupled canopy structure dynamic and radiative transfer models to estimate biophysical canopy characteristics. *Remote Sensing of Environment*, *95*(1), 115–124.

Koetz, B., Morsdorf, F., Sun, G., Ranson, K. J., Itten, K., & Allgower, B. (2006). Inversion of a lidar waveform model for forest biophysical parameter estimation. *IEEE Geoscience and Remote Sensing Letters*, *3*, 49–53.

Koetz, B., Schaepman, M., Morsdorf, F., Itten, K., & Allgöwer, B. (2004). Radiative transfer modeling within a heterogeneous canopy for estimation of forest fire fuel properties. *Remote Sensing of Environment*, *92*(3), 332–344.

Kvalseth, T. O. (1985). Cautionary note about r^2. *American Statistician*, *39*, 279–285.

Lauber, K., & Wagner, G., (1996). Flora helvetica. flora der schweiz. Bern, Stuttgart, Wien, Paul Haupt Verlag, 1613.

Lefsky, M. A., Cohen, W. B., Acker, S. A., Parker, G. G., Spies, T. A., & Harding, D. (1999). Lidar remote sensing of the canopy structure and biophysical properties of douglas-fir western hemlock forests. *Remote Sensing of Environment*, *70*, 339–361.

Lovell, J., Jupp, D., Culvenor, D., & Coops, N. (2003). Using airborne and groundbased ranging lidar to measure canopy structure in australian forests. *Canadian Journal of Remote Sensing*, *29*(5), 607–622.

Means, J. E., Acker, S. A., Fitt, B. J., Renslow, M., Emerson, L., & Hendrix, C. (2000). Predicting forest stand characteristics with airborne scanning lidar. *Photogrammetric Engineering and Remote Sensing*, *66*(11), 1367–1371.

Morsdorf, F., Meier, E., Kötz, B., Itten, K. I., Dobbertin, M., & Allgöwer, B. (2004). Lidar-based geometric reconstruction of boreal type forest stands at single tree 26 level for forest and wildland fire management. *Remote Sensing of Environment*, *3*(92), 353–362.

Myneni, R., Nemani, R., & Running, S. (1997). Estimation of global leaf area index and absorbed par using radiative transfer models. *IEEE Transactions on Geoscience and Remote Sensing*, *35*, 1380–1393.

Næsset, E. (2002). Predicting forest stand characteristics with airborne scanning laser using a practical two-stage procedure and field data. *Remote Sensing of Environment*, *80*(1), 88–99.

Næsset, E. (2004). Effects of different flying altitudes on biophysical stand properties estimated from canopy height and density measured with a small-footprint airborne scanning laser. *Remote Sensing of Environment*, *91*(2), 243–255.

Ni-Meister, W., Jupp, D. L. B., & Dubayah, B. (2001). Modeling lidar waveforms in heterogeneous and discrete canopies. *IEEE Transactions on Geoscience and Remote Sensing*, *39*(9), 1943–1958.

Nobis, M., & Hunziker, U. (2005). Automatic thresholding for hemispherical canopy photographs based on edge detection. *Agricultural and Forest Meteorology*, *128*(3–4), 243–250.

Riano, D., Meier, E., Allgöwer, B., Chuvieco, E., & Ustin, S. L. (2003). Modeling airborne laser scanning data for the spatial generation of critical forest parameters in fire behavior modeling. *Remote Sensing of Environment*, *86*(2), 177–186.

Riano, D., Valladares, F., Condes, S., & Chuvieco, E. (2004). Estimation of leaf area index and covered ground from airborne laser scanner (lidar) in two contrasting forests. *Agricultural and Forest Meteorology*, *124*(3–4), 269–275.

Schlerf, M., & Atzberger, C. (2006, Feb.). Inversion of a forest reflectance model to estimate structural canopy variables from hyperspectral remote sensing data. *Remote Sensing of Environment*, *100*(3), 281–294.

Smolander, S., & Stenberg, P. (2003, Dec.). A method to account for shoot scale clumping in coniferous canopy reflectance models. *Remote Sensing of Environment*, *88*(4), 363–373.

Sun, G., & Ranson, K. (2000). Modeling lidar returns from forest canopies. *IEEE Transactions on Geoscience and Remote Sensing*, *38*(6), 2617–2626.

Watson, D. J. (1947). Comparative physiological studies in the growth of field crops. I. Variation in net assimilation rate and leaf area between species and varieties, and within and between years. *Annals of Botany*, *11*, 41–76.

Weiss, M., Baret, F., Smith, G. J., Jonckheere, J., & Coppin, P. (2004). Review of methods for in situ leaf area index (lai) determination: Part II. Estimation of lai, errors and sampling. *Agricultural and Forest Meteorology*, *121*(1–2), 37–53.

White, M. A., Asner, G. P., Nemani, R. R., Privette, J. L., & Running, S. W. (2000). Measuring fractional cover and leaf area index in arid ecosystems: Digital camera, radiation transmittance, and laser altimetry methods. *Remote Sensing of Environment*, *74*(1), 45–57.

Wotruba, L., Morsdorf, F., Meier, E., & Nüesch, D. (2005). Assessment of sensor characteristics of an airborne laser scanner using geometric reference targets. *International Archives of Photogrammetry and Remote Sensing*, *XXXVI*(3/W19), 1–6.

Yu, X., Hyyppä, J., Kaartinen, H., & Maltamo, M. (2004). Automatic detection of harvested trees and determination of forest growth using airborne laser scanning. *Remote Sensing of Environment*, *90*, 451–462.

Zoller, H. (1992). *Vegetationskarte des schweizerischen nationalparks und seiner umgebung.* Hallwag AG: Bern.

Zoller, H. (1995). Vegetationskarte des schweizerischen nationalparks. erläuterungen. *National Park Forschung*, *108*.